Abrasion and Nanoscratch in Nanostructured Epoxy Coatings

Stefano Turri, Luca Torlaj, Francesca Piccinini, Marinella Levi

Dipartimento di Chimica, Materiali e Ingegneria Chimica "Giulio Natta," Politecnico di Milano, Piazza Leonardo da Vinci 32, 20133 Milan, Italy

Received 2 September 2009; accepted 7 February 2010
DOI 10.1002/app.32309
Published online 7 June 2010 in Wiley InterScience (www.interscience.wiley.com).

ABSTRACT: A series of epoxy nanostructured coatings based on diglycidyl ether of bisphenol A (DGEBA) and an isophorone diamine crosslinker was prepared. Top-down nanocomposites (3% nanofiller) were obtained by the mechanical dispersion of nanoalumina, silanized nanoalumina, and organomodified clays. Bottom-up hybrids were instead achieved after the silanization of the DGEBA resin and after cocrosslinking with tetraethylorthosilicate through a self-catalyzed sol–gel process. The curing process of the nanocomposites was studied by differential scanning calorimetry and suggested an overall increase in the crosslinking kinetics in the presence of nanoparticles. Other characterization included dynamic mechanical analysis, Buchholtz indentation hardness testing, and Taber abrasion testing. Finally, atomic force microscopy (AFM) techniques were used to study the surface morphology of the coatings and to produce nanoscratches. We concluded that, in the top-down nanocomposites, there were minor changes in the surface hardness and a slight improvement in the abrasion resistance, whereas the nanoscratch resistance assessed by AFM tests showed significantly better performances in the hybrid coatings obtained through sol–gel chemistry. © 2010 Wiley Periodicals, Inc. J Appl Polym Sci 118: 1720–1727, 2010

Key words: atomic force microscopy (AFM); coatings; nanocomposites

INTRODUCTION

Epoxy coatings are widely used for their ease of application, excellent hardness and adhesion to many substrates, good chemical resistance, and low cost.[1] Several examples of nanostructured epoxy materials have been reported in recent years. Classical top-down nanocomposites are based on mechanical high-energy dispersion processes of different small particles, such as organomodified clays, nanooxides, carbon nanotubes, and polyhedral oligomeric silsesquioxanes.[2] Nanooxides and clays are among nanofillers that have a lower cost and a wider industrial availability. Moreover, they allow the preparation of high-optical-clarity coatings when they are properly dispersed.

It was reported that the introduction of low-aspect-ratio nanooxide particles can moderately increase the Young modulus and fracture toughness in epoxy nanocomposites,[3] up to 40%. Photoactive nanooxides, such as ZnO or TiO_2, have also been used to obtain clear coatings with improved UV light screening and resistances and higher refractive indices.[4,5] Hard ceramic nanoparticles can also be used to increase wear resistance;[6] in such a case, the effective surface functionalization of the nanoparticle is needed to prevent three-bodied abrasion mechanisms and to achieve better chemical adhesion with the polymer matrix.

The microstructure and degree of exfoliation in clay-based epoxy coatings is widely dependent on the processing conditions and on the choice of the curing agent. The formation of mixed intercalated–exfoliated structures improves both the Young modulus and impact strength[7] (up to around +140%) because the high-aspect-ratio clay platelets significantly hinder crack propagation.[8,9] Less information is available on the tribological properties of clay-based epoxies, but a slight improvement (30%) in the abrasion resistance was reported.[10]

Epoxy hybrids based on sol–gel chemical processes have been described, too, but to a lesser extent. Highly homogeneous interpenetrating hybrid morphologies were obtained with low contrast images, even with electron microscopy.[11,12] As far as tribological properties are concerned, a clear reduction in the coefficient of friction was reported for SiO_2 containing sol–gel hybrids.[11]

In this study, the attention was given to the examination of the surface mechanical properties of epoxy-nanostructured materials. In particular, an industrial product used for civil and industrial flooring was used as a base resin because the main requirements of the specific application were a high

Correspondence to: S. Turri (stefano.turri@polimi.it).
Contract grant sponsor: Regione Lombardia, Metadistretto NanoVer ID 4086.

TABLE I
Coating Compositions and T_g Values of Different Epoxy Nanocomposites

Materials	Component A	Component B	Method	Inorganic content (% w/w)	T_g (°C)
Std	DGEBA	Isophorone diamine	–	0	100
Std + Al_2O_3	DGEBA	Isophorone diamine	Dispersion	3	91
Std + Al_2O_3-*g*	DGEBA	Isophorone diamine	Dispersion	3	94
Std + CL30B	DGEBA	Isophorone diamine	Dispersion	3	98
Rs	DGEBA + APTES	–	Sol–gel	0	93
Rs + SiO_2–sol	DGEBA + APTES	TEOS/H_2O/EtOH	Sol–gel	5	142

resistance to scratches and abrasion. Both top-down nanocomposites based on the mechanical dispersion of nanoalumina and organoclay and bottom-up hybrids obtained through the sol–gel polycondensation of silanized epoxies were prepared and considered. The surface mechanical properties of the resulting materials were, in particular, investigated by exploration of existing correlations among the measurements of abrasion resistance on the macroscale and nanoscratch hardness through atomic force microscopy (AFM) techniques.

EXPERIMENTAL

Materials

The base resin used in this study was an epoxy bicomponent product based on diglycidyl ether of bisphenol A (DGEBA) as component A and a cycloaliphatic diamine hardener (isophorone diamine) diluted with benzyl alcohol as component B. The product was kindly supplied by Alcea S. R. L. (Senago, Italy), and it is a standard (Std) product used for civil and industrial flooring. The unfilled product is indicated in the following text as Std, see Table I.

The nanofillers AluC (nano-Al_2O_3 from Degussa, Essen, Germany) and Cloisite 30B (CL30B; an organophilic montmorillonite clay from Southern Clays, Austin, Texas) were used without any further purification. All other chemicals were commercially available grades of glycidoxypropyltrimethoxysilane and 3-aminopropyltriethoxysilane (APTES), tetraethylorthosilicate (TEOS; 99% pure), ethanol (EtOH; 99% pure), and benzyl alcohol, all purchased from Aldrich (Saint Louis, MI), and deionized water.

Sample preparations and curing conditions

Nanocomposites

AluC and CL30B fillers were first mixed with DGEBA by ultrasonication in a ultrasonic bath (Starsonic 90 (Liarre s.r.l., Bologna, Italy), 40°C for 30 min), followed by mechanical ultradispersion at 9000 rpm for 60 min (Ultraturrax T25, Ika Werke GmbH, Staufen, Germany). In some cases, the nanoalumina was previously surface-grafted in the liquid phase with glycidoxypropyltrimethoxysilane, according to procedures reported in the literature.[13] The corresponding coatings are indicated by the suffix -*g*. The final nanocomposite materials were prepared in all cases by the mixture of components A and B in proper stoichiometric ratios (100 : 60 by weight as indicated by the supplier); then, the mixture was bar-coated on various substrates (e.g., glass, steel) and cured with the following cycle: 2 h at ambient temperature, 2 h at 50°C, and 2 h at 120°C. The final coating thickness against steel was measured by the magnetic induction method with a Deltascope FPM instrument, Helmut Fischer GmbH (Sindelfingen-Maichingen, Germany) and was around 200–400 μm.

Sol–gel hybrids

For sol–gel-based hybrids, the DGEBA resin was first derivatized with APTES in a 1 : 2 molar ratio to form an epoxy adduct bearing alkoxy silane end groups, as shown in Figure 1.

We made this adduct by simply pouring together for 2 h the reagents in a glass vessel, which was kept under nitrogen and gentle stirring for 8 h. Such an adduct and the corresponding self-crosslinked

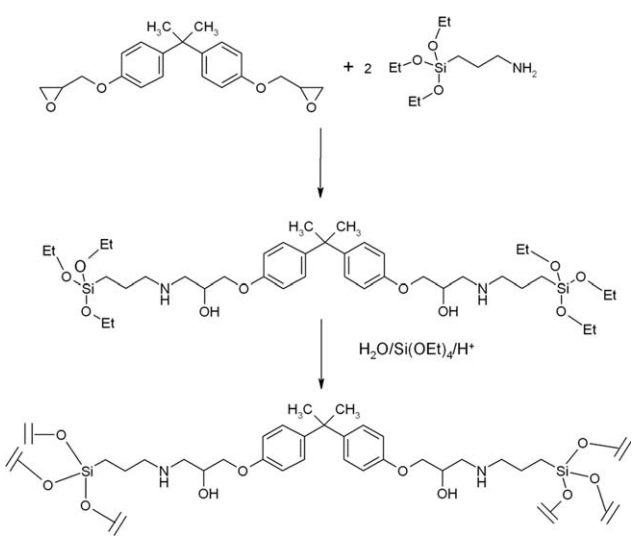

Figure 1 Scheme of the sol–gel reaction occurring between DGEBA, APTES, and TEOS.

coating are indicated as Rs in the following text. Separately, a sol was prepared by the mixture of TEOS, water, and EtOH at a molar ratio of 1 : 3 : 4.5, and such a formulation was then blended with the Rs-silanized epoxy in an amount corresponding to a theoretical silica content of 5 wt % to obtain a sol–gel epoxy hybrid. No external catalysis was used because the basicity of the Rs adduct was enough to promote hydrolysis and the condensation reaction of silicon alkoxides. The coating was bar-applied onto glass and steel substrates and cured with the following cycle: 2 h at ambient temperature, 2 h at 50°C, and 2 h at 120°C. The final coating thickness was between 5 and 15 μm. At higher thicknesses, extensive cracking of the film was observed.

All of the compositions of the nanocomposites and sol–gel hybrid epoxies are reported in Table I.

CHARACTERIZATION

Differential scanning calorimetry (DSC) analyses were carried out with a Mettler Toledo DSC 823[e] instrument (Im langacher, Switzerland). The following cycles were used to measure the extent of crosslinking and the glass-transition temperature (T_g) in the epoxy coatings: heating from 20 to 250°C, cooling from 250 to 20°C, and heating again from 20 to 200°C, always at a rate of 20°/min. In the first scan, the enthalpy peak of the reaction was integrated to calculate the corresponding conversion–temperature curve. T_g was measured as the half- heat capacity (C_p) value of the transition detected after the third scan. Moreover, the activation energy (E_a) of the crosslinking reaction was studied after heating scans at different heating rates (q's; 5, 10, 20, and 30°/min) by measurement of the peak temperature for each scan according to the Kissinger and Ozawa theories.[14]

Dynamic mechanical analysis (DMA) measurements were carried out with a Mettler Toledo DMA/SDTA861[e] instrument in tensile mode with dynamic scans from −50 to 200°C at a frequency of 1 Hz after we determined the linear viscoelastic range of the sample (deformation < 0.5%).

Other mechanical tests consisted of the Buchholtz indentation hardness test, according to ISO 2815, and abrasion resistance testing by the Taber tests, according to ISO 7784.

X-ray diffraction analysis were performed with a Philips PW 1710 diffractometer (Amsterdam, Holland) with Cu Kα radiation (wavelength (λ) = 1.5406 Å). The range of 2θ scans was 2–15°. The basal spacing (d) of the clay was estimated from the 001 peak in X-ray diffraction according to the Bragg's law:

$$\lambda = 2d_{hkl} \sin\theta$$

where d is the interplaner distance, hkl are the Miller indices, θ is diffraction angle.

AFM topography and demodulation images were acquired in tapping mode with an Nscripton DPN instrument (Nanoink, Chicago, IL). Si_3N_4 probes from Pacific Nanotechnology (Santa Clara, CA) were used with a force constant of 42 N/m and a nominal frequency of 320 kHz. The scan conditions were chosen according to Maganov et al.[15] to get stiffness contrast in the phase image, which means that the bright features were stiffer phases than the dark ones.

Nanometric scratches were produced on the coating surfaces again by AFM at a constant force with the same tip used for the AFM measurements. Calibration of the tip sensitivity was performed under the same conditions used for the experiments carried out on a standard hard silicon surface. This value could be used to convert the deflection data (in volts) to a force value (nano-Newtons).[15] A constant force of 3400 nN was applied on the AFM cantilever during scratching. With a first approximation assumed to have a conical shape of the AFM tip, the scratch hardness (H_s) may be defined as follows:

$$H_s = \frac{4F}{\pi w^2} \tag{1}$$

where F is the normal load applied on the AFM tip and w is the width of the scratch.[16,17]

RESULTS AND DISCUSSION

Processing

The effect of the nanofillers on the processing of the bicomponent epoxies was studied by DSC thermal analysis. Because the crosslinking of an epoxy–polyamine system is a polyaddition-type reaction, there is no mass but only heat exchange, and the DSC data could be used for a quantitative modeling of crosslinking process with the assumption that heat flow was proportional to the extent of the reaction (α). The following equations were used to calculate α and the rate of conversion ($d\alpha/dt$) from the integrated enthalpy peaks; ΔH_{tot} is the normalized total heat of the reaction (J/g) released from the 20÷250 heating scan of the unfilled epoxy, and dH_t is the heat exchanged in the dt interval:

$$\alpha_t = 1/\Delta H_{tot} \int (dH_t/dt)dt \tag{2}$$

$$[d\alpha/dt]_t = 1/\Delta H_{tot}[dH_t/dt]_t \tag{3}$$

where t is time.

By comparing the conversion curves of the Std resin (Fig. 2) with the those of nanocomposites, we envisaged some slight differences, especially in the temperature range between 50 and 100°C, where an accelerating effect due to presence of nanofillers

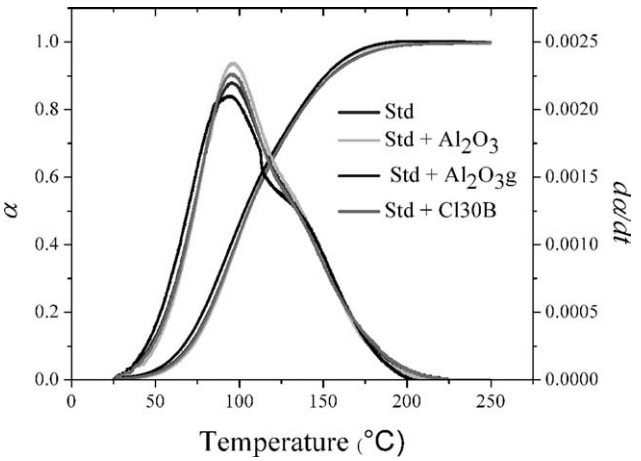

Figure 2 Comparison of α and $d\alpha/dt$ values of different nanocomposites and Std resin with temperature.

was seen. Some better analysis was done by the observation of the $d\alpha/dt$–temperature differential curves, as shown again in Figure 2. Also, in this case, it was possible to see that the maximum exothermal temperature peaks for the nanocomposites were quite similar to those of the Std coating. As far as the CL30B-clay-based nanocomposite was concerned, a small accelerating effect was attributed to the presence of $-NR_4^+$ and —OH groups of the organic modifier, which could act as catalysts of the epoxy–amine crosslinking reaction, as reported by Seo and Kim[18] for similar systems. Moreover, in the same cases, chemical interactions can also be present, as in the case of silane-grafted alumina, which leads to a general increase in the epoxy group content and, thus, to a partially unbalanced stoichiometry. Actually, the peak temperature curve of the epoxy filled with grafted alumina seemed to occur at a temperature (T) lower than for the Std resin. Although the differences were quite small, by observing the $d\alpha/dt$–temperature curves in the range between 50 and 100°C, we observed that the grafted alumina (darker line) led to an acceleration of the curing process compared to the ungrafted one (brighter line).

DSC scans at various q values were used to estimate E_a of the reaction according to the Ozawa and Kissinger equations, respectively:[14]

$$E_a = -2.3R\{(d\log q)/[d(1/T_p)]\} \quad (4)$$

$$E_a = -2.3R\left\{\left(d\log\left(q/T_p^2\right)\right)/[d(1/T_p)]\right\} \quad (5)$$

where T_p is the temperature of the maximum exothermal peaks and R is the Universal gas constant. The results of the data fitting according to the model reported previously are summarized in Table II, whereas some examples are shown in Figure 3.

TABLE II
E_a Values Calculated with the Ozawa and Kissinger Equations

	E_a (kcal/mol)	
Materials	Ozawa model	Kissinger model
Std	52.9	46.8
Std + Al_2O_3	56.8	50.6
Std + Al_2O_3-*g*	58.3	52.1
Std + CL30B	60.2	53.0

The presence of nanofillers slightly increased the temperature dependence of the crosslinking reaction in the epoxy–amine formulations; the experimental E_a values were comparable to those reported by Xu et al.[19] for unfilled epoxy resins.

The X-ray diffraction technique was then used to investigate the structure of the clay-based nanocomposites. As shown in Figure 4, the diffraction pattern of pristine CL30B in comparison to the 3% clay-filled epoxy nanocomposite differed in both position and intensity of the 2θ peaks. In particular, the 001 peak reflection shifted from 2θ = 2.5° to 2θ = 5.2°; this corresponded to a d-spacing increase from 18.5 to 34.9 Å and suggested the formation of

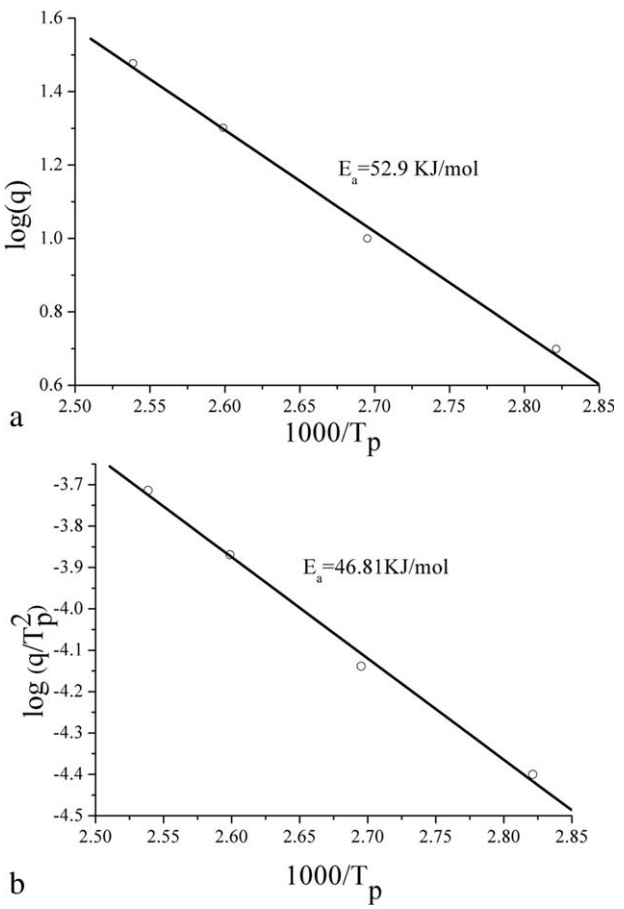

Figure 3 E_a values calculated with the (a) Ozawa and (b) Kissinger equations.

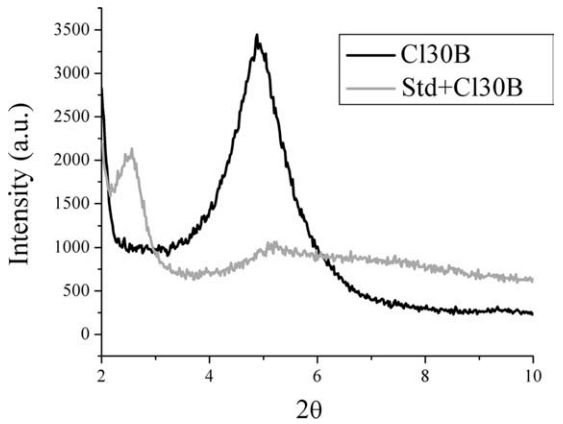

Figure 4 Diffraction patterns of CL30B and the Std + CL30B nanocomposite.

predominantly intercalated nanocomposites. The minor intensity peak around 5.5° in the nanocomposite may have been due to a small fraction of unintercalated or even slightly flocculated clay.

Mechanical properties of the composites

Some examples of the DMA curves of the epoxy nanocomposites are shown in Figure 5, whereas all the main numerical results are reported in Table III. The effect of the presence of nanofillers on the storage modulus (E') in the glassy state was weak, whereas hybrid coatings from sol–gel processes appeared significantly softer. DMA allowed the estimate of the density of crosslinking (ν) with the assumption that $E' = 3G'$ (storage shear modulus) in the rubbery plateau ($T = 140$°C); according to the ideal rubber theory,[20] the results are reported in Table III:

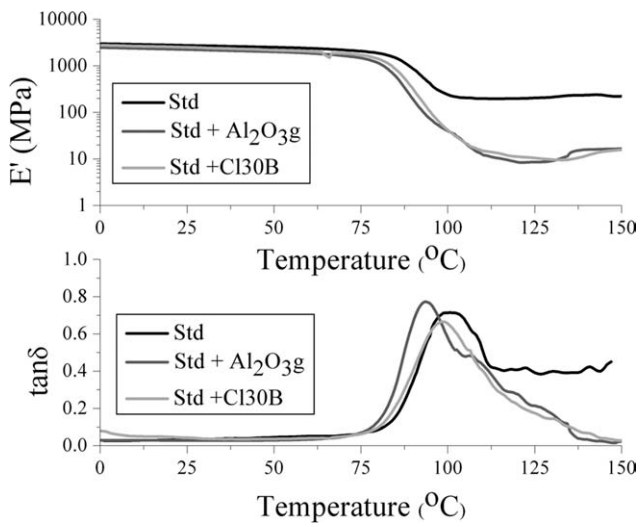

Figure 5 E' and tanδ behavior of some epoxy nanocomposites.

TABLE III
E' Values at 23 and 140°C, ν, and $\tan\delta_{max}$ for Different Nanocomposites

Materials	E' (MPa) at 23°C	E' (MPa) at 140°C	ν (mmol/cm^3)	$\tan\delta_{max}$
Std	2785	236	2.13×10^{-2}	100.5
Std + Al_2O_3	2610	8	3.95×10^{-4}	91.0
Std + Al_2O_3-*g*	2265	16	9.28×10^{-4}	93.5
Std + CL30B	2540	12	9.65×10^{-4}	99.0
Rs	1550	136	1.69×10^{-2}	92.5
Rs + SiO_2–sol	1570	265	1.22×10^{-2}	140.0

$\tan\delta_{max}$ is the temperature corresponding to the maximum tanδ.

$$\sigma = G(\lambda - 1/\lambda^2) = \nu RT(\lambda - 1/\lambda^2) \quad (6)$$

where σ is the tensile stress, G is the shear modulus, and λ is the elongation.

As shown from data in Table III, the densities of crosslinking for all of the nanocomposites were significantly smaller than for the Std resin. A similar behavior was already observed in polyurethane nanocomposite coatings[21] and was attributed to the possible chemical reactivity of the nanofillers, which involved a slight stoichiometric embalancement. The ν values obtained with the sol–gel hybrids were comparable with those of the Std resin, but, of course, in this case, both the chemical structure and the crosslinking mechanism were completely different.

Table IV reports the indentation hardness values (Buchholtz hardness) and the Taber abrasion resistance values of the epoxy coatings considered. A significant improvement in the wear index was achieved with the introduction of grafted alumina and especially clay; actually, the weight loss was much lower than for the Std coating. Interestingly, similar results were observed for the sol–gel hybrids, although the results were less reliable, because, in the latter case, a sufficiently thick sample preparation for the test was very difficult. As far as hardness was concerned, this property was marginally influenced by the nanofillers. The abrasion and

TABLE IV
Indentation Hardness and Wear Index from the Taber Test of the Epoxy Nanocomposite Coatings

Materials	Indentation hardness	Wear index (mg/kcycle)
Std	99 ± 2	63 ± 15
Std + Al_2O_3	101 ± 7	75 ± 13
Std + Al_2O_3-*g*	97 ± 7	56 ± 5
Std + CL30B	98 ± 3	33 ± 5
Rs	75 ± 9	27 ± 12
Rs + SiO_2–sol	87 ± 11	35 ± 7

TABLE V
Surface Roughness Data

Materials	R_a (nm)	R_{ms} (nm)
Std	0.16 ± 0.02	0.21 ± 0.03
Std + Al_2O_3	0.59 ± 0.04	0.86 ± 0.06
Std + Al_2O_3-*g*	1.24 ± 0.04	1.46 ± 0.05
Std + CL30B	3.15 ± 0.04	5.05 ± 0.08
Rs	0.13 ± 0.01	0.20 ± 0.03
Rs + SiO_2–sol	2.65 ± 0.09	4.69 ± 0.14

surface hardness behavior seemed not to be closely related properties.

AFM characterization

The surface morphologies of the nanocomposites were examined by means of AFM. The changes in the surface topography were determined quantitatively by the mean surface roughness (R_a) and root mean square (R_{ms}) values. This analysis is usually done when the surfaces are characterized by a degree of randomness.[22] The roughness calculation is based on the determination of a median surface level for the image and then the evaluation of the standard deviation within the image. Table V summarizes the surface roughness values of such selected compositions.

The unfilled resin exhibited the smallest roughness values, whereas coatings containing grafted alumina and organic clay showed the highest ones.

In Figure 6, the demodulation phase images are shown for nanocomposites obtained after the high-energy mechanical dispersion of nanooxides {Std unfilled epoxy [Fig. 6(a)], epoxy filled with 3% Al_2O_3-*g* ([Fig. 6(b)], and, by the chemical sol–gel processes [Fig. 6(c)], Std+CL30B and Rs+SiO_2–sol [Fig. 6(d)]). In the phase-contrast images, the small bright (hard) domains were attributed to the inorganic phase, whereas the dark (soft) domains belonged to the polymeric network. In particular, Figure 6(b–d) shows that the organic and inorganic phases were fully interconnected with no major macroscopic phase separation occurring during the crosslinking process. The silica domains generated by the sol–gel process [Fig. 6(d)] were fully embedded in the polymeric matrix and showed a nanometric domain size in the range 30–40 nm, with some larger moieties.

Nanometric scratches were made on each sample. For example, Figure 7(a–d) shows topographic images of nanoscratches obtained at constant force on the Std, Std+Al_2O_3-*g*, Std+CL30B, and Rs+SiO_2–sol (5% SiO_2) coatings, respectively. A large pileup was observed in all cases, which was less evident

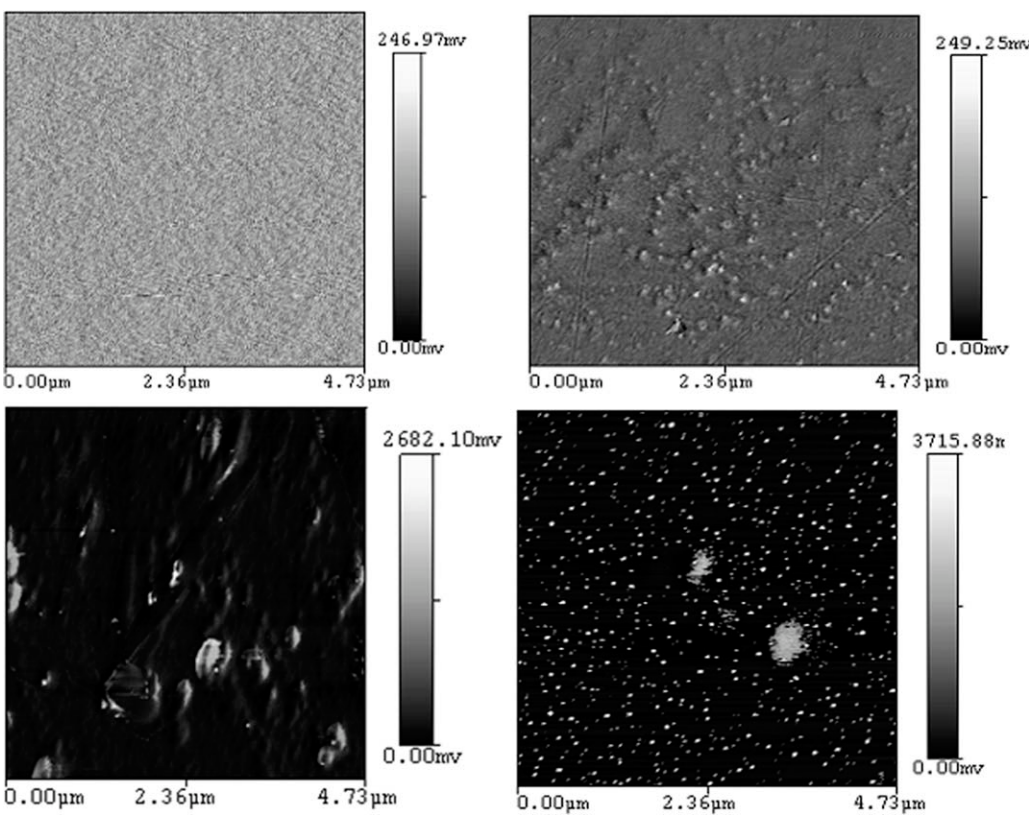

Figure 6 Phase images performed on (a) Std, (b) Std+Al_2O_3-g, (c) Std+CL30B, and (d) Rs+SiO_2–sol.

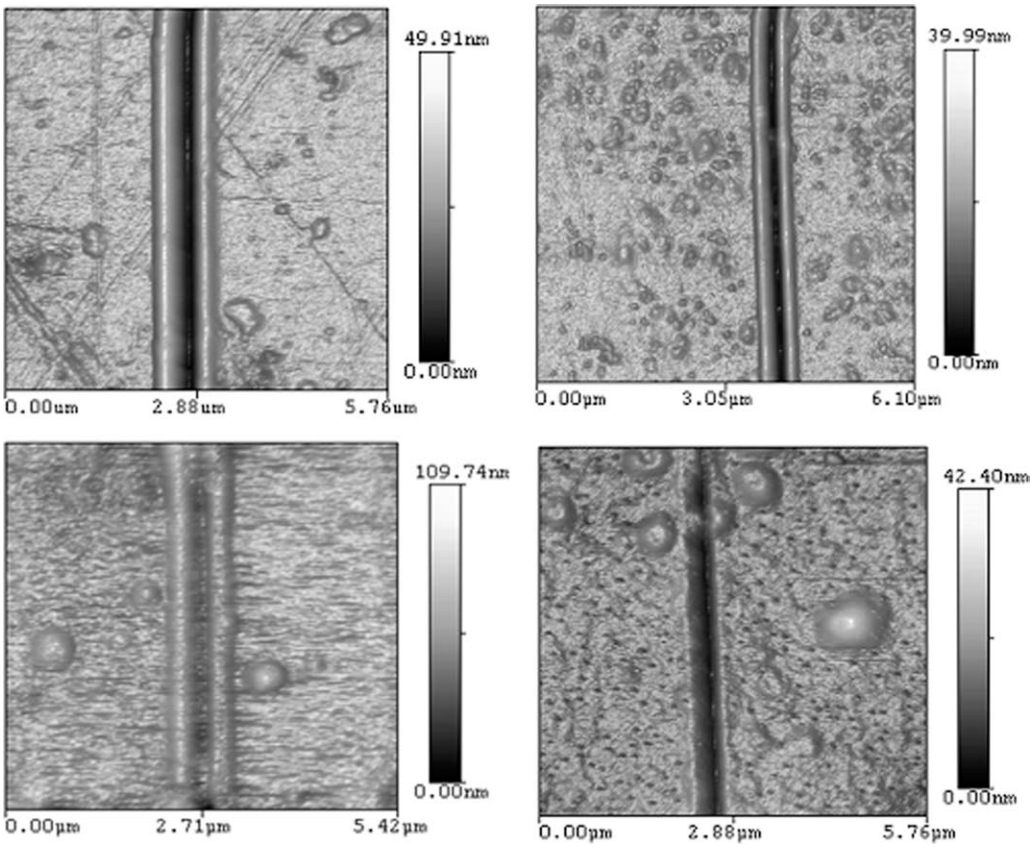

Figure 7 Topographic images of the nanoscratch analysis performed on (a) Std, (b) Std + Al_2O_3-g, (c) Std+CL30B, and (d) Rs+SiO_2–sol (5% SiO_2) coatings.

for the sol–gel hybrids; this indicated ductile deformation.

In Table VI, all of the scratch depths and w values are reported. We observed a large improvement in the scratch resistance (i.e., smaller scratches) in the nanostructured samples. Scratch depths for the Std epoxy coatings were approximately 19 nm, whereas for the materials containing clays (Std + CL30B), they were as low as 14 nm. Interestingly, samples obtained with the sol–gel methods showed very small scratches, as low as 7–9 nm. Table VI summarizes also the dynamic H_s values calculated for each sample according to eq. (1). The presence of nanoparticles in the nanocomposite materials led to a significant improvement in the scratch resistance. The best result in this respect was reached by the dispersion of the surface-modified particles, such as grafted Al_2O_3 and the organoclays. For the samples from the sol–gel processes, we observed that the presence of 5% silica led to values of H_s as high as 784 MPa, which was, by far, higher than those achieved by any of the top-down nanocomposite coatings.

TABLE VI
Scratch Depth, w, and H_s Values

Materials	Scratch depth (nm)	w (nm)	H_s (MPa)
Std	19.21 ± 0.92	319.3 ± 11.4	42.8 ± 3.2
Std + Al_2O_3	17.99 ± 0.59	228.8 ± 4.3	83.1 ± 3.1
Std + Al_2O_3-g	15.17 ± 0.22	151.4 ± 5.8	190.4 ± 14.3
Std + CL30B	14.14 ± 0.82	196.9 ± 4.9	112.3 ± 5.6
Rs	9.12 ± 0.11	168.9 ± 2.9	152.5 ± 5.2
Rs + SiO_2–sol	6.94 ± 0.33	74.6 ± 2.5	783.6 ± 51.6

CONCLUSIONS

A standard bicomponent epoxy was modified by both the introduction of nanoparticles and by cocrosslinking in a sol–gel-based formulation. The surface mechanical behavior was studied by both abrasion and nanoscratch resistance tests. In the latter case, an AFM technique was used to produce and measure scratches. In general, a significant improvement in H_s was observed, with the best results obtained in the case of epoxies modified with silanized oxide nanoparticles, in particular, with sol/gel hybrids. A more detailed investigation of the scratch behavior by AFM considering the effect of tip speed, applied force, and possible viscoelastic recovery is needed to further investigate scratch mechanisms at a nanometric scale and to determine a correlation

with the macroscopic surface mechanical behavior of coatings.

The authors thank Lucio Carlucci (Alcea) for his help and the stimulating discussions.

References

1. Wicks, Z. W. In Organic Coatings Science and Technology; Wiley: New York, 1994.
2. Kickelbick, G. Prog Polym Sci 2003, 28, 83.
3. Naous, W.; Yu, X.; Zhang, Q.; Naito, K.; Kagawa, Y. J Polym Sci Part B: Polym Phys 2006, 44, 1466.
4. McCook, N. L.; Boesl, B.; Burris, D. L.; Sawyer, W. G. Tribol Lett 2006, 22, 253.
5. Guan, C.; Lu, C.; Liu, Y.; Yang, B. J Appl Polym Sci 2006, 102, 1631.
6. Basara, C.; Yilmazer, U.; Bayram, G. J Appl Polym Sci 2003, 98, 1081.
7. Liu, T.; Tjiu, W. C.; Tong, Y.; He, C.; Goh, S.; Chung, T. S. J Appl Polym Sci 2004, 941, 1236.
8. Kornmann, X.; Thomann, R.; Muhlhaupt, R.; Finter, J.; Berglund, L. A. Polym Eng Sci 2002, 42, 1815.
9. Jia, Q. M.; Zheng, M.; Xu, C. Z.; Chen, H. X. Polym Adv Technol 2006, 17, 168.
10. Qi, C.; Gao, H.; Yan, F.; Liu, W.; Bao, G.; Sun, X.; Chen, J.; Zheng, X. J Appl Polym Sci 2005, 97, 38.
11. Liu, Y.; Lin, Y.; Chen, C.; Jeng, R. J Appl Polym Sci 2003, 90, 4047.
12. Lu, S. R.; Zhang, H.; Zhao, C.; Wang, X. J Appl Polym Sci 2005, 40, 1079.
13. Vassileva, E.; Friedrich, K. J Appl Polym Sci 2003, 89, 3374.
14. Prime, R. B. In Thermal Characterization of Polymeric Materials; Turi, E. A., Ed.; Academic: Orlando, FL, 1981; p 532.
15. Maganov, S. N.; Elings, V.; Whangbo, M. H. Surf Sci Lett 1997, 375, 385.
16. Briscoe, B. J.; Pelillo, E.; Sinha, S. Polym Eng Sci 1996, 30, 2996.
17. Williams, J. A. Tribol Int 1996, 29, 675.
18. Seo, K. S.; Kim, D. S. Polym Eng Sci 2006, 46, 1318.
19. Xu, W.; Bao, S.; Shen, S.; Wang, W.; Hang, G. Part A: Polym Chem J Polym Sci 2003, 41, 378.
20. Treloar, L. R. G. The Physics of Rubber Elasticity, 3rd ed.; Oxford University Press: Oxford, 1975.
21. Turri, S.; Alborghetti, L.; Levi, M. J Polym Res 2008, 15, 365.
22. Lu, S.; Zhang, H.; Zhao, C.; Wang, X. J Appl Polym Sci 2006, 101, 1075.